LA-UR-05-7953

Active Piezoelectric Sensing for Damage Identification in Honeycomb Aluminum Panels

R. Andrew Swartz[1], Eric Flynn[2], Daniel Backman[3], R. Jason Hundhausen[4], Gyuhae Park[5]

[1]Department of Civil and Environmental Engineering, University of Michigan, Ann Arbor, MI 48109

[2]Division of Engineering and Applied Sciences, California Institute of Technology, Pasadena, CA 91125

[3]Department of Mechanical Engineering, Ohio State University, Columbus, OH 43210

[4]Engineering Sciences and Applications, Weapon Response Group, MS T001, Los Alamos National Laboratory, Los Alamos, NM 87545

[5]Engineering Sciences and Applications, Engineering Institute, MS T001, Los Alamos National Laboratory, Los Alamos, NM 87545

ABSTRACT

This paper presents a novel approach for Lamb wave based structural health monitoring (SHM) in honeycomb aluminum panels. Piezoelectric transducers are utilized as both sensors and actuators for Lamb wave propagation. In this study, a suite of four signal processing algorithms are employed and grouped into one package to improve the damage detection capability. The signal processing algorithms used include wavelet attenuation, correlation coefficients of power density spectra, triangulation of reflected waves, and time reversal acoustics. These SHM algorithms are built into a MatLab interface that integrates and automates the hardware and software operations and displays the results for each algorithm to the analyst for side by side comparison. The effectiveness of each of these signal processing algorithms for SHM in honeycomb aluminum panels under a variety of damage conditions is then investigated.

1. INTRODUCTION

The aerospace industry is increasingly utilizing honeycomb aluminum sandwich panels in a variety of applications. One application that is of particular interest to military planners is for unmanned aerial vehicles (UAVs), which are often constructed using a honeycomb panel skin (Figure 1). The honeycomb panels used in this study are constructed from two thin aluminum face sheets bonded to an aluminum honeycomb core; the face sheets carry nearly all of the bending loads whereas the core material supports the transverse shear loads. This configuration produces a panel that has a significantly higher strength to weight ratio than would a solid panel of the same material composition; however, given the distribution of loads in such panels, any damage to these panels can lead to a marked and substantial decrease in their load-carrying capability. Potential types of damage include cracking, buckling of the face sheets, buckling of the core, and delamination of the face material from the core. Potential sources of damage include overloading, foreign object impacts, corrosion, manufacturing defects, and fatigue [1]. According to the Government Accountability Office (GAO), the Department of Defense spends $15.3 million for a single Global Hawk UAV [2] and $3.3 million for a Predator UAV [3]. Given the high cost of replacement for a

Figure 1: Predator UAV – (Photo Courtesy of the Department of Homeland Security).

UAV, as well as the critical nature of the missions these vehicles perform, the availability of real-time information regarding the condition and serviceability of the aircraft is vital.

SHM is the process of measuring the dynamic response of a system and determining from these data the current state of the system's "health" in near real time. This process is typically carried out by comparing the dynamic response of an undamaged, baseline structure to that of the current, potentially damaged structure. The advantages of SHM include the possible detection of damage at its onset, before it has had a chance to propagate and potentially cause catastrophic failure if left unchecked [4]. In this paper, Lamb wave based SHM techniques are investigated for honeycomb aluminum panels. Some of these techniques are very similar to previous work performed by Lee and Staszewski [5], and Kessler, et al. [6] on the subject of Lamb wave propagation in metallic structures and carbon composites, respectively, as well as work by Park, et al. [7] involving impedance methods.

Lamb waves are coupled longitudinal and shear waves of plane strain within a plate that propagate in a variety of symmetric and antisymmetric modes. To use Lamb waves for SHM, it is useful to have a waveform that is easily recognizable both before and after propagation through the plate. Lamb waves are dispersive in nature, meaning that different frequency components travel at different velocities within the plate [8]. To maximize the effectiveness of the SHM technique, it is useful to choose a driving frequency for which the various Lamb wave modes are temporally well spaced and at which the modes of interest are relatively non-dispersive. Choosing the proper driving frequency allows the receiving sensors to record the input signal with a minimal amount of interference.

In this study, a MatLab-based user interface called H.O.P.S. (health of plate structures) was created, which allows the analyst to configure the data acquisition system and display the results from each of four damage identification algorithms for side by side comparison. This side by side comparison of results simplifies the task of identifying the relative effectiveness and sensitivity of each algorithm. A brief description of the four algorithms used in H.O.P.S. follows; a more detailed explanation of each method is described in section 2. The first method is based on a comparison of Lamb wave attenuation in a baseline undamaged (i.e., "healthy") plate to that of a damaged plate test case; the second method uses a cross-correlation of the power spectral density of the recorded response in the baseline condition to that of the test case; the third method attempts to identify Lamb waves reflected from the point of damage and locate them using time-of-flight and triangulation; and the final method employs a time reversal algorithm to identify nonlinearities in the panel. An important goal in all four algorithms is to be able to detect damage on the side opposite the transducers, because it is likely that, in an aerospace application, the transducers will be mounted on the inside of the aircraft, while damage is much more likely to occur on the outside.

2. EXPERIMENTAL SETUP AND PROCEDURES

2.1. Setup

The panels tested in this study are composed of two aluminum face sheets bonded to an aluminum honeycomb core. The panels have dimensions of 609.6 mm (24 inches) square. Two panels are studied: one with a thickness of 6.35 mm (0.250 inches) and one with a thickness of 12.7 mm (0.500 inches). The dimensional properties of the two panels are summarized in Table 1. The panels are suspended vertically by elastic cords during testing. The panels are instrumented with a regular array of 12.7 mm diameter-circular PZT transducers. The 6.35 mm thick panel has a four by four (sixteen total) array of transducers spaced 180 mm apart in each direction, evenly spaced from the edges (Figure 2(a, b, d)). The 12.7 mm thick panel has a three by three (nine total) array of transducers, also spaced 180 mm apart in each direction, which allows a greater edge distance for the outer PZT transducers (Figure 2(c)). The PZT transducers are bonded to a single side of each panel using a quick-setting adhesive. Lamb wave data are acquired using a commercial system that has a sampling frequency up to 25 MHz. The SHM algorithms for both hardware and signal processing are written in MatLab. These algorithms control the entire process through the graphical user interface (GUI). An external amplifier (Krohn-Hite 7602M) is used to amplify the input signal to the PZT actuators.

In order to simulate damage in a reversible manner, industrial putty is affixed to the face of the panel in sizes ranging from 800 mm^2 to 1200 mm^2 (Figure 2(e)). The damage identification methods are attempted for putty

placed on the same side of the panel as are the piezoelectric transducers, as well as on the opposite side (Figure 3(a)). Multiple damage locations are also simulated using two pieces of putty, placed both on the sensor side as well as both on the opposite side. Multiple site damage is also simulated by simultaneously placing the industrial putty on both sides of the panel. Damage is also simulated using a cylindrical-neodymium magnet with diameter 38 mm, a mass of 152g, and that is capable of exerting a maximum force of 423N. The magnet is placed on the side opposite the sensors and a 25 mm by 51 mm rectangular plate is placed opposite the magnet on the sensor side, (Figure 3(b)). Irreversible damage is inflicted on the panel by pressing a 6.35 mm square steel rod into the face of the panel. The load on the steel rod is increased to create larger and larger areas of damage. The damage is applied slowly in order to prevent breaking or debonding of the PZT patches. To simulate more extreme damage scenarios, a screwdriver is used to create holes in the panel, first through only the face sheet opposite the sensors, then through the entire panel, shown in Figures 8 and 9.

Table 1: Panel Dimensional Data.

Plate Thickness (mm)	Cell Diameter (mm)	Density (kg/m^3)	Face Sheet Thickness (mm)
6.35	9.53	529	0.508
12.7	12.7	36.8	0.813

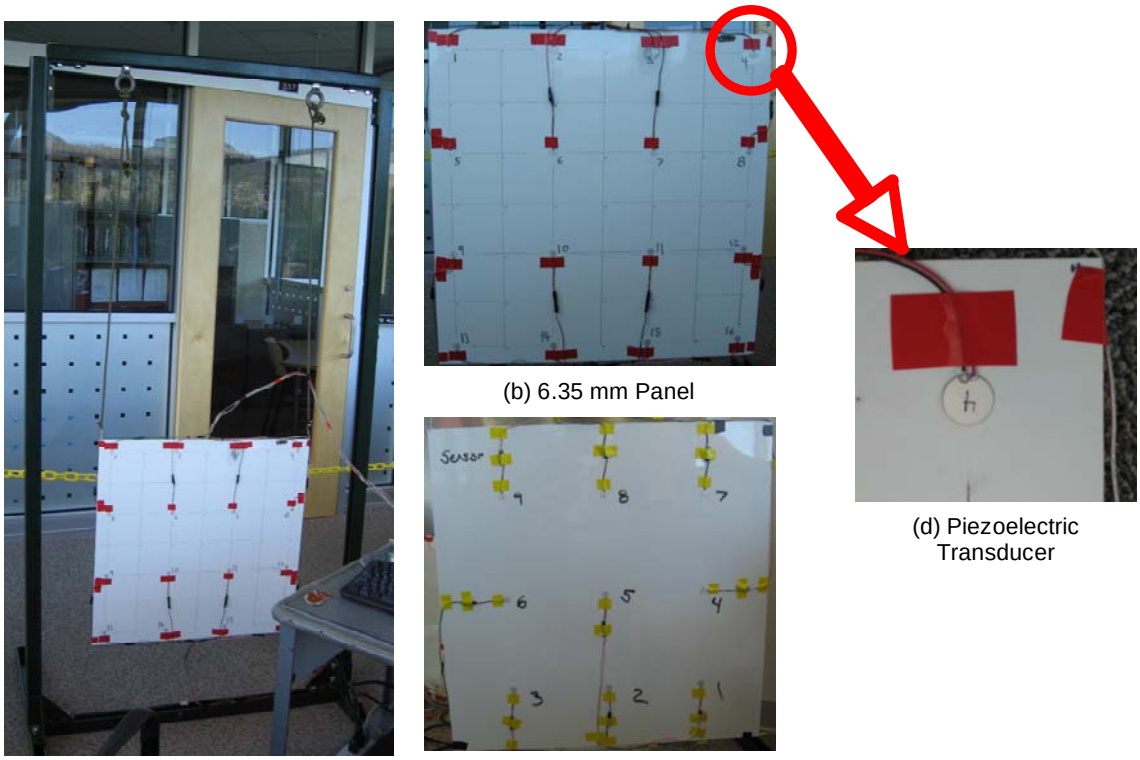

(a) Panel Support Condition

(b) 6.35 mm Panel

(c) 12.7 mm Panel

(d) Piezoelectric Transducer

Figure 2: Experimental Setup.

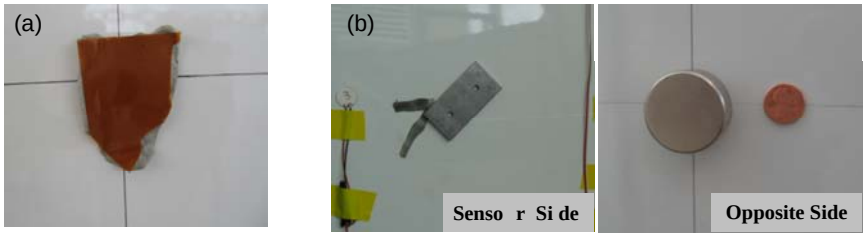

Figure 3: Simulated Damage for Algorithm Testing: (a) Putty; (b) Magnet and Plate.

2.2. Signal Processing Algorithms

Four signal processing algorithms are explored in this paper for use in SHM of honeycomb aluminum panels. The algorithms are written as MatLab functions and integrated by use of a MatLab GUI. The system is designed to communicate automatically with the data acquisition system, integrating the software and hardware components of the SHM system. Descriptions of the four algorithms follow.

2.2.1. Wavelet Attenuation

The first SHM technique presented in this paper takes advantage of the attenuation of Lamb waves. As Lamb waves propagate through a plate, the mechanical energy is dissipated through various processes that cause a decrease in the magnitude of the wave. The amount of attenuation between any two points in the plate will change when damage is introduced on the path between them. A comparison of the baseline signal and the test case yields the condition of the panel. This Lamb wave attenuation technique is based on that described by Sohn, et al [8] for detection of delaminations in composite structures.

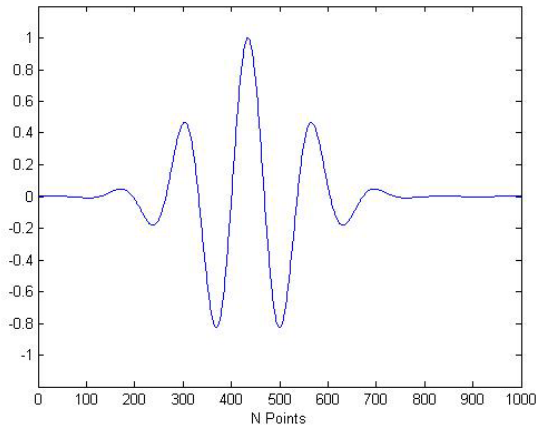

Figure 4: Input Morlet Wavelet.

The input waveform is a five-peak Morlet wavelet (Figure 4). The experimentally derived driving frequency is 200 kHz in the 6.35 mm panel and 250 kHz in the 13.7 mm panel. These produce a well separated, non-dispersive S_0 mode. In this case, the S_0 mode at the input frequency is used for damage detection because it is the fastest wave mode and therefore, less susceptible to interference with reflected waves from the edge of the panel [6]. To achieve a better attenuation comparison between the baseline and test signals, both signals are transformed using the wavelet transformation. A more accurate wavelet transform is achieved by using a wavelet basis function that is the same as the input wave [9, 10]. The wavelet transform is given by

$$Wf(u,s) = \int_{-\infty}^{\infty} f(t) \frac{1}{\sqrt{s}} \psi^*_{u,s}(t)dt \,, \tag{1}$$

where *u* refers to the translations and *s* refers to the dilations of the mother wavelet, defined by

$$\psi^*_{u,s} = \frac{1}{\sqrt{s}} \psi(\frac{t-u}{s}). \tag{2}$$

The result of performing this operation yields the time-frequency response of the recorded signal. Only the component of the input driving frequency is of interest. The time response at the input frequency is recorded for both the baseline case and the test case. A comparison is made by use of a damage index (DI) based on a ratio of the kinetic energy of the test signal to that of the baseline signal (Equation 3).

$$DI = \left| \frac{\int_{u0}^{u1} Wf_t(u, s_0)du - \int_{u0}^{u1} Wf_b(u, s_0)du}{\int_{u0}^{u1} Wf_b(u, s_0)du} \right| \tag{3}$$

In Equation 3, subscripts *b* and *t* stand for the baseline and test signals respectively, and u_0 and u_1 stand for the starting and ending time points for the first recorded S_0 mode. The DI ranges from zero, undamaged, and increases to a maximum value of one as the amount of attenuation increases. A more comprehensive description of this technique can be found in Sohn, et al [8]. An appropriate damage threshold must be selected that will separate damaged path signals from undamaged signals. For this study, a threshold value of three standard deviations above the baseline-baseline damage index is experimentally derived.

Once the damaged pathways between each of the piezoelectric transducer pairs are determined, they are plotted on a predefined grid. The total number of damaged paths intersecting each grid point is divided by the total number of undamaged paths intersecting that grid point. That result is normalized over the entire grid. The grid must be coarse enough to provide an adequate number of sensor path intersections for each element (Figure 5). The normalized values are plotted on the grid in the H.O.P.S. user interface to indicate the most likely locations of damage to the panel (Figure 6).

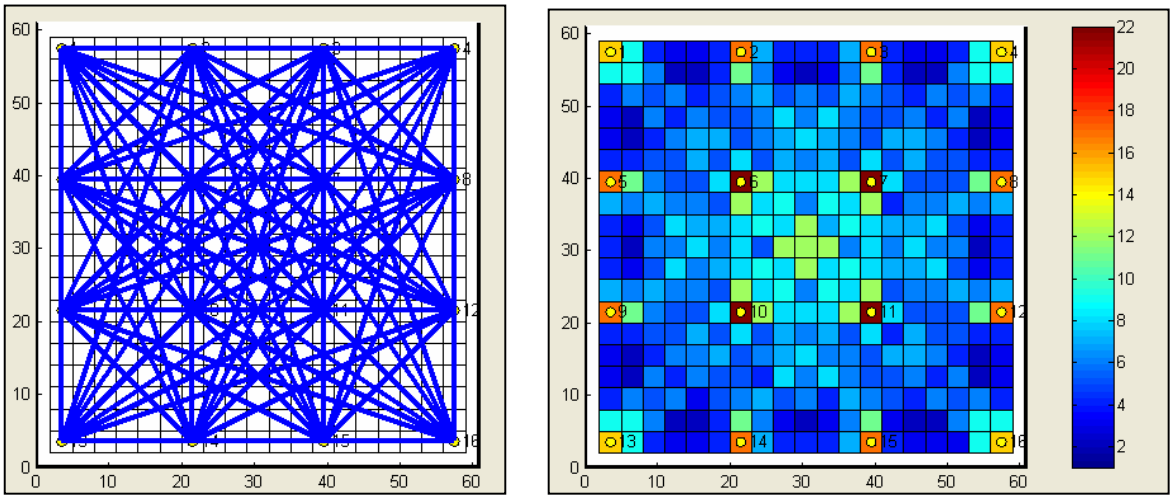

Figure 5: Damage Location Grid with Path Crossings.

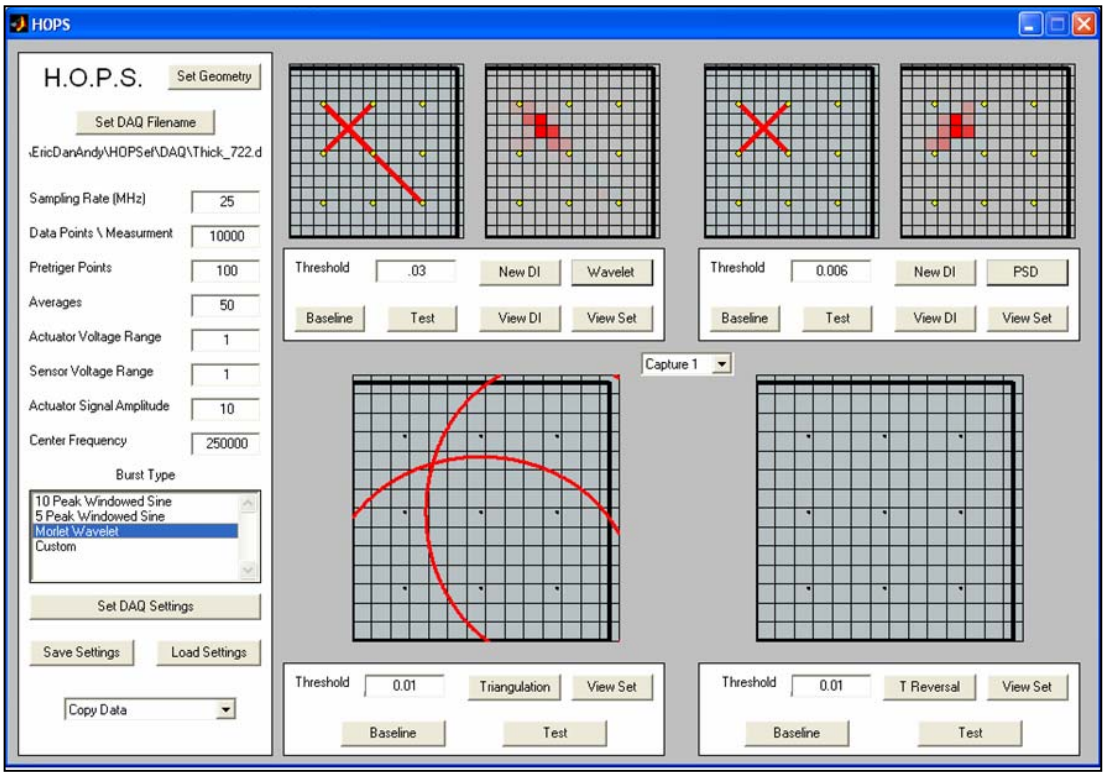

Figure 6: H.O.P.S. Graphical User Interface.

2.2.2. Cross-correlation of Power Spectral Density

A second technique employed for feature extraction from the recorded Lamb wave data involves the cross-correlation of the power spectral density (PSD) functions between the baseline and the test case signals. The same Morlet wavelet that is used in the Lamb wave attenuation method is propagated through the panels. A second signal consisting of a sine sweep from 50 kHz to 300 kHz is also explored. The propagated signal is recorded for every piezoelectric transducer pair path and the power spectral density for each of those signals is calculated. Although the panel is being actuated at only one driving frequency, the frequencies of the resulting Lamb waves are dependent on the thickness of the panel. Subtle variations in the panel thickness and the bond between the face sheets and core create different frequency components in the signal that is ultimately recorded, resulting in a frequency rich signal from which a useful PSD can be calculated. The damage index is based on the correlation coefficient of the PSD for the baseline signal versus the PSD of the test signal in a range around the driving frequency. In this case, it is between the frequencies of 50 kHz and 300 kHz. For consistency, the correlation coefficient is subtracted from one so that the signals with the highest correlation (i.e., indicate the least damage) have damage indices that approach zero, while signals with less correlation, indicating greater degrees of damage, will have greater damage indices, with a maximum DI value of one.

Once damage indices have been assigned to each path, a damage threshold is required to distinguish damaged path signals from the undamaged path signals. In the case of the cross-correlation of PSDs, a value of three standard deviations above the baseline-baseline damage index is considered damaged. The same grid and path based damage location algorithm is used for this method as is used for the Lamb wave attenuation method.

2.2.3. Triangulation of Reflected Waves

The third method for damage identification that is investigated utilizes the waves reflected from damage in the panel. As Lamb waves propagate through a panel, they interact with defects in the structure, reflecting from the defect boundaries. These reflections are recorded by the piezoelectric transducers. A comparison between the test case and the baseline data reveals the presence and time location of the reflected waves in the recorded signal. Time-of-flight can be used to for a wave of known velocity to determine the distance between the sensor and the defect. Using data from an array of sensors, the location of the defect can be triangulated.

The same baseline and test signals recorded for the wavelet method are used for this method; however, only data recorded at the transducers in the corner positions of the array are used. The signals are first processed using the Wavelet transform and the time response for the driving frequency is isolated in the same manner as for the wavelet algorithm. A Hilbert transform is then performed on the resulting signals to minimize the effects of minor phase changes. The resulting signals are subtracted from each other leaving only the differences between the two signals. This result is normalized between zero and one with zero representing the case of no change between the baseline and test signals. A threshold value is determined below which changes are considered to be noise, not damage. Peaks that occur before and during the normal first wave arrival are not considered as possible reflection candidates.

The damage is then located using the time-of-flight data. The first point at which the normalized difference signal exceeds the threshold value is identified as the first arrival of waves deflected from the damage boundary. This is recorded as the time-of-flight for the reflected waves. The program calculates the wave velocity using the distance between actuating and sensing transducers, and the time between actuation of the signal and the arrival of the fundamental symmetric mode wave. The possible paths for the reflected wave define an ellipse around the sensing transducer according to Equation 4.

$$x(\omega) = \frac{d^2 - p^2}{2(d\cos(\omega) - p)} \tag{4}$$

Where *d* is the distance between the actuator and the sensor, *p* is the path length traveled by the reflected wave, *w* is an angle that ranges from zero to 180 degrees, and *x* is the distance to the sensor. These ellipses are plotted for each of the corner transducers. The intersection of these ellipses defines the damaged area.

2.2.4. Time Reversal Acoustics

Time reversal acoustics (TRA) are useful for identifying nonlinear damage. The process of time reversal acoustics is to reconstruct the original input signal at the original actuator by propagating the time reversed response from the original sensor. As long as the structure is linear, the signal (theoretically) can be reconstructed perfectly. Any nonlinearities in the system, including those resulting from damage will cause the reconstructed signal to differ from the original signal. However, time reversal acoustics is not useful for identifying damage that does not create nonlinear responses in the system because the original signal can be reconstructed perfectly despite the damage. In both the 6.35 mm and 12.7 mm panels, the time reversal algorithm is capable of reconstructing the original signal in all the damaged cases considered, pointing out that the simulated damage cases are not too inherently nonlinear. It also exhibits reduced sensitivities compared to other methods described earlier (in the case that TRA is used without baselines). Furthermore, because of noise in the acquisition system, as well as inherent nonlinearities in the honeycomb aluminum panel, the TRA is not substantially investigated in this study and is left as a future study.

3. RESULTS

3.1. Wavelets

The attenuation of the fundamental symmetric mode is found to be sensitive to both simulated damage as well as real damage. This method produces the greatest difference between the damaged case and the baseline case for simulated damage in the form of industrial putty on the sensor side of the panel (Figure 7). Sensor paths crossing the putty produce damage indices as large as 0.68. This method is less sensitive to putty on the opposite side of the panel from the sensors; in this case, the largest damage indices are on the order of 0.23. However, it is still possible to discern the damaged paths from the undamaged paths. Similar results are obtained for the case of simulated damage caused by the magnet and plate. Real damage is introduced into the panel incrementally. For both panels, eight damage increments of increasing severity are used (Figures 8 and 9). The damage ranges from small face wrinkles (one to three cm in diameter) to large face wrinkles causing delamination of the honeycomb structure (up to eight cm in diameter) to holes through the back face and finally through the entire panel. The resulting damage indices along each path are summarized in Figure 10 for the 12.7 mm panel; results for the 6.35 mm panel are similar.

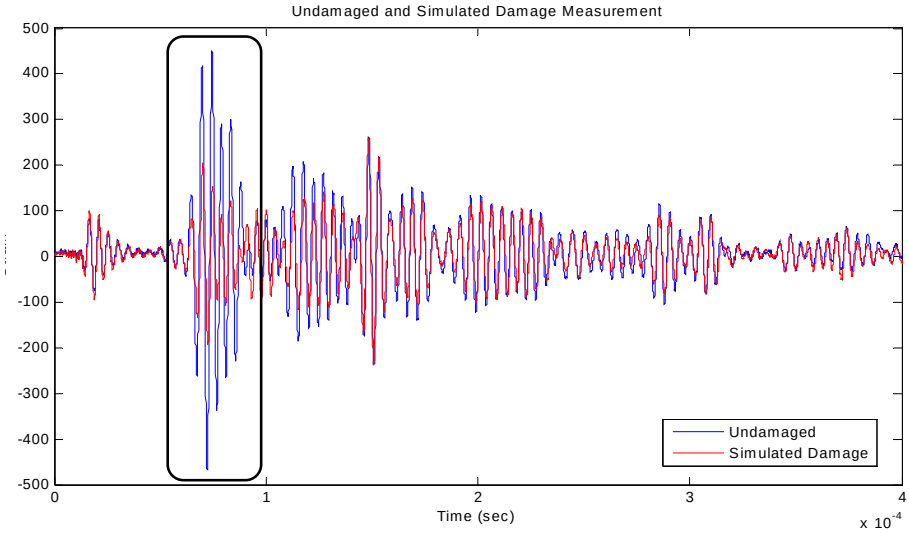

Figure 7: Large Attenuation Damage for Putty on Sensor Side of Panel.

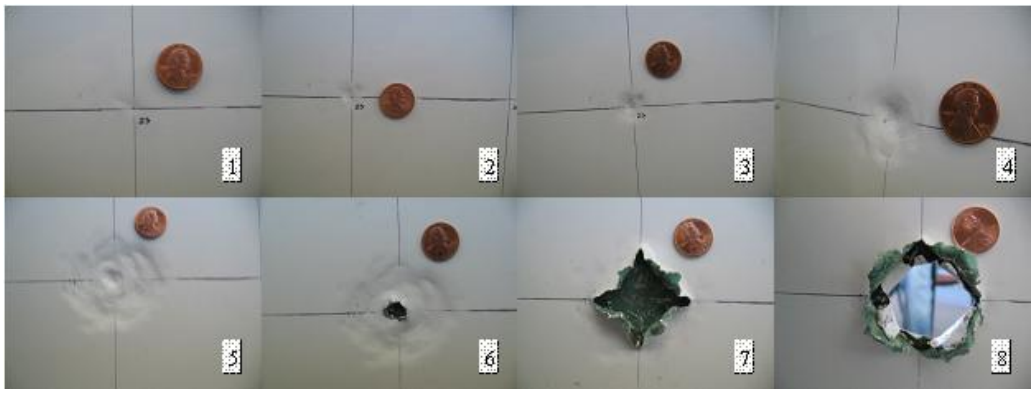

Figure 8: 6.25 mm Panel Damage Cases 1-8.

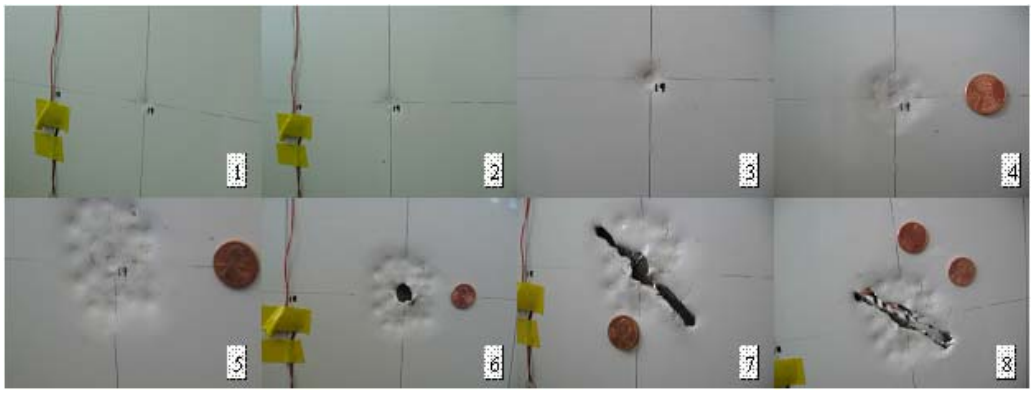

Figure 9: 12.7 mm Panel Damage Cases 1-8.

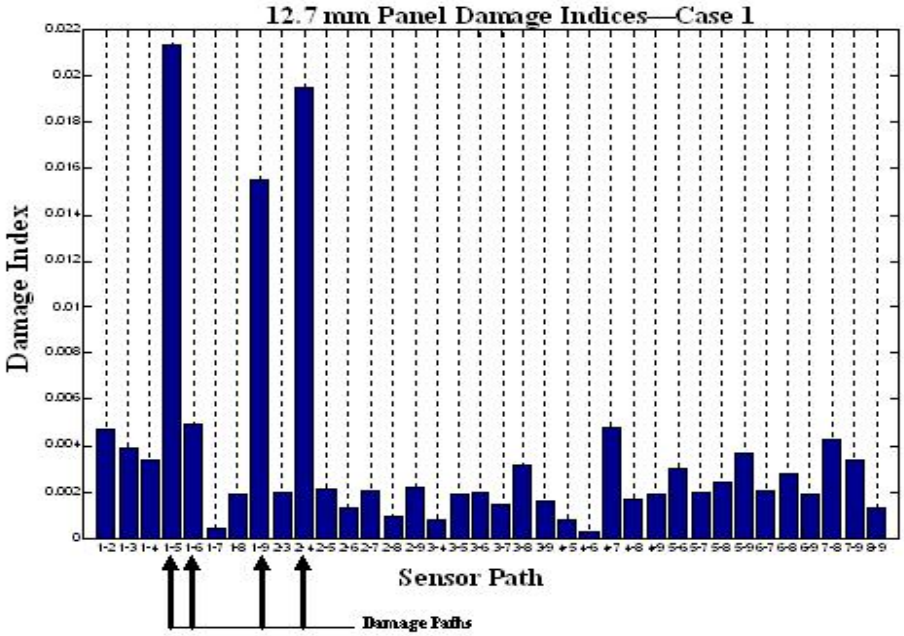

Figure 10: Comparison of Sensor Path Damage Indices – Damage Case 1.

For face wrinkling damage (cases one through five), the damage index is more sensitive to increases in the diameter of the wrinkle than increases in its depth. This is evident from the relatively large jump in the DI between damage cases one and two where the wrinkle is enlarged laterally and the lack of a jump in the DI between cases two and three where the depth of the wrinkle is increased. The DI actually drops when the first hole is created in the opposite side face sheet but increases again as the hole size increases. The largest damage indices are measured for case eight when the hole is propagated through the entire thickness of the plate.

The damage location algorithm successfully identifies the damaged paths. A summarization of the mean damage indices for damaged and undamaged cases is shown in Figure 11. These paths are then used to locate the damage on a user-defined grid. The grid size used for this study is 30 mm by 30 mm. The state of damage for a given grid location is indicated by the intensity of the color displayed, which is a function of the probability that that grid is damaged. The probability is based on the number of damaged paths intersecting the grid location versus the number of undamaged grid lines. The locations for the 12.7 mm panel of the calculated damage versus actual damage for each panel are shown in Figure 12. Similar results are obtained for the 6.35 mm panel. Note that the damage index for the damage paths does not always increase as damage increases.

3.2. Cross-Correlation of Power Spectral Density

The power spectral density function cross-correlation shows changes when simulated damage is applied to the panel as well as large face wrinkles and holes; however, it is less sensitive to small face wrinkles. In the 12.7 mm plate for damage cases five through eight (large face wrinkles and holes), the damage indices range between 0.03 and 0.09 for damaged paths and between 0.00 and 0.02 for the undamaged cases. These ranges allow for easy separation of damaged and undamaged paths by use of the damage index threshold value. Cases one through four (small face wrinkles), however, have damage indices ranging between 0.62 and 0.85 for damaged paths and between 0.08 and 0.65 for undamaged paths. The overlap makes it difficult to effectively separate the damaged paths from the undamaged paths. Damage indices for the 12.7 mm panel for damage cases two and seven are presented in Figure 13(a) and Figure 13(b) respectively. The mean damage indices for the damaged paths using the cross-correlation of PSD are plotted for the 12.7 mm panel as a function of damage case in Figure 14.

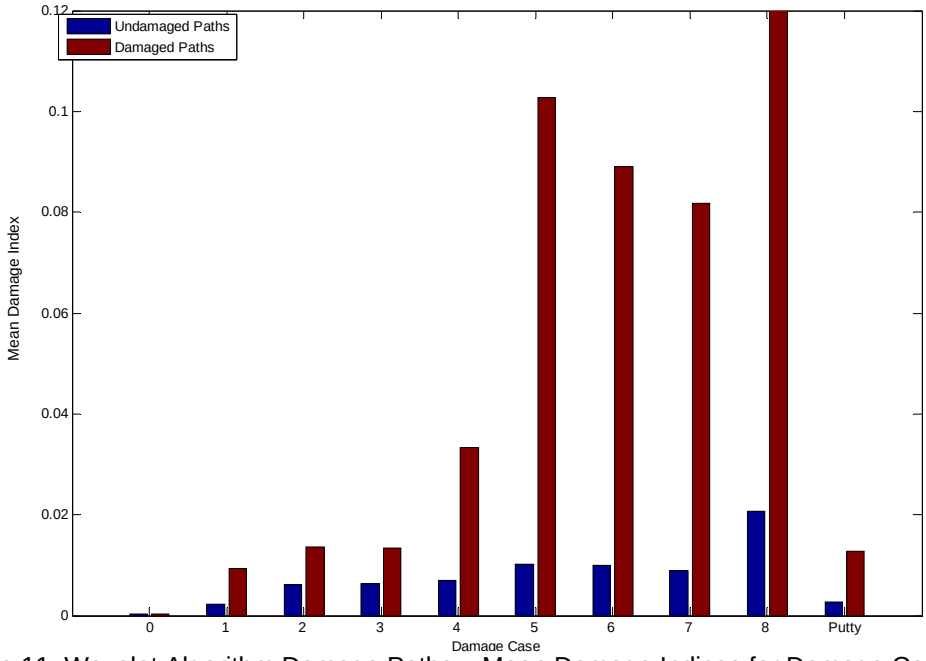

Figure 11: Wavelet Algorithm Damage Paths – Mean Damage Indices for Damage Cases 1-8.

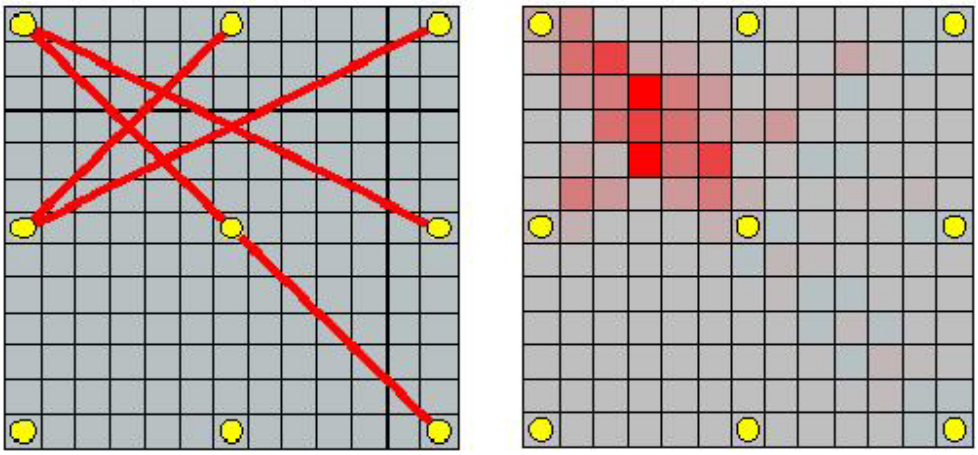

Figure 12: Wavelet Algorithm Damage Paths for Damage Case 7.

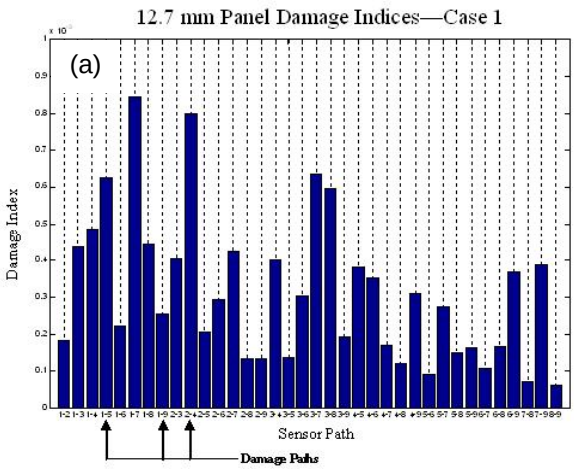

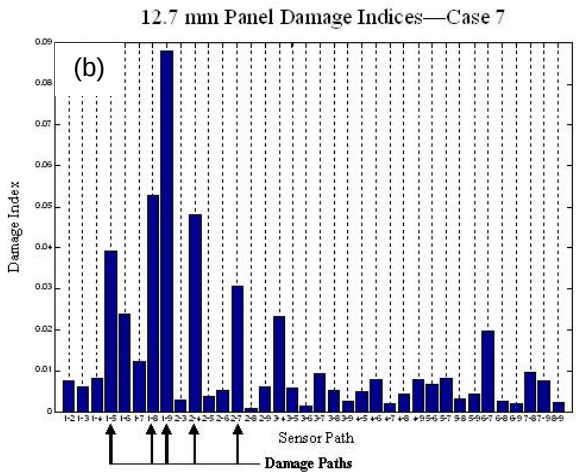

Figure 13(a): Noisy Damage Indices, Damage Case 1. Figure 13(b): Damage Indices, Damage Case 7.

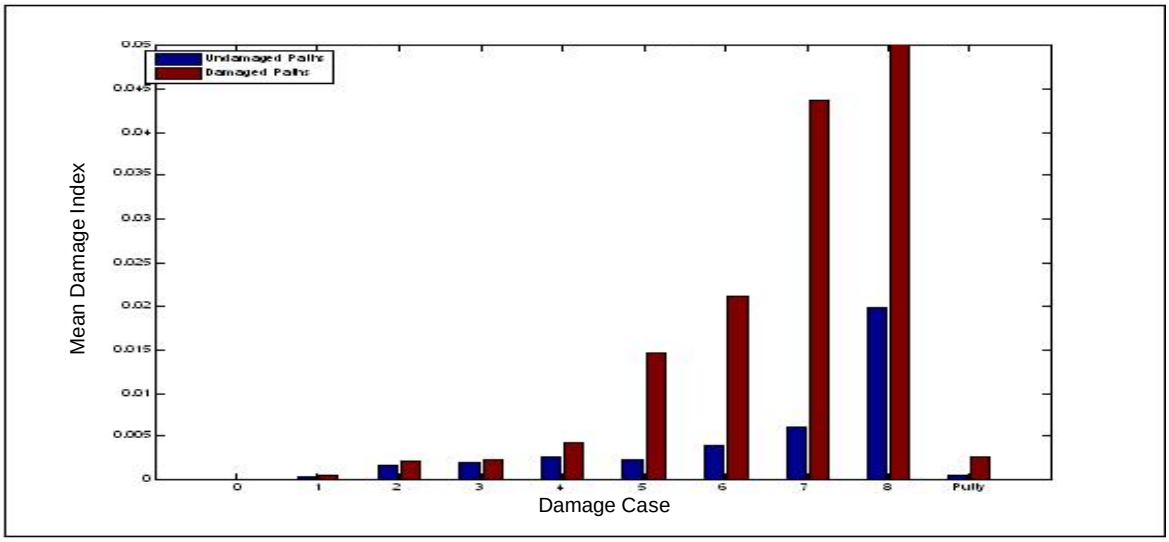

Figure 14: Cross-Correlation of PSD Damage Paths – Mean Damage Indices for Damage Cases 1-8.

Damage indices for the 6.35 mm panel show still less separation between the damaged and undamaged paths. The damage location is calculated using the same algorithm as is used for the wavelet method. In cases where the damaged paths are distinguishable from the undamaged paths, the algorithm is able to locate the damage. Where there is little or no separation between damage indices, the algorithm fails. Though this method is less effective at locating damage as the wavelet attenuation method, the PSD damage indices increase reliably as damage increases making this method more effective at characterizing the degree of damage.

One problem with the current implementation of this algorithm is that because the power spectral density is calculated over the entire length of the signal, reflections from the damage boundaries create differences in not only the damaged path signals, but the undamaged path signals as well. This means that as damage is introduced into the plate, the power spectral density of the damaged path signals change resulting in increases in the damage indices, but so do the signals for the undamaged paths. This drives up the damage indices for the undamaged paths as well, potentially leading to false positives along undamaged paths. Also investigated is the use of a sine sweep signal because it has more frequency content than just a simple Morlet wavelet. The sine sweep does not produce noticeable improvements in the ability of the algorithm to identify damage.

3.3. Reflected Signal Triangulation

The algorithm for damage identification using signals reflected from damage boundaries is sensitive to holes in the face sheets, but less sensitive to face wrinkling and delamination. The damage indices for damage cases 1-5 are not significantly different than those for the baseline signal (Figure 15). It is not until holes are created in the panels, that the reflections become evident in the test case signal (Figure 16). The location algorithm calculates a wave velocity of 498 m/s in the 12.7 mm panel for the fundamental symmetric Lamb wave mode and 462 m/s in the 6.35 mm panel, based on the arrival time and the distance between transducers. Using that velocity and Equation 4, the location of the damage is triangulated and can be seen as the intersection of the ellipses surrounding the sensors in Figure 17.

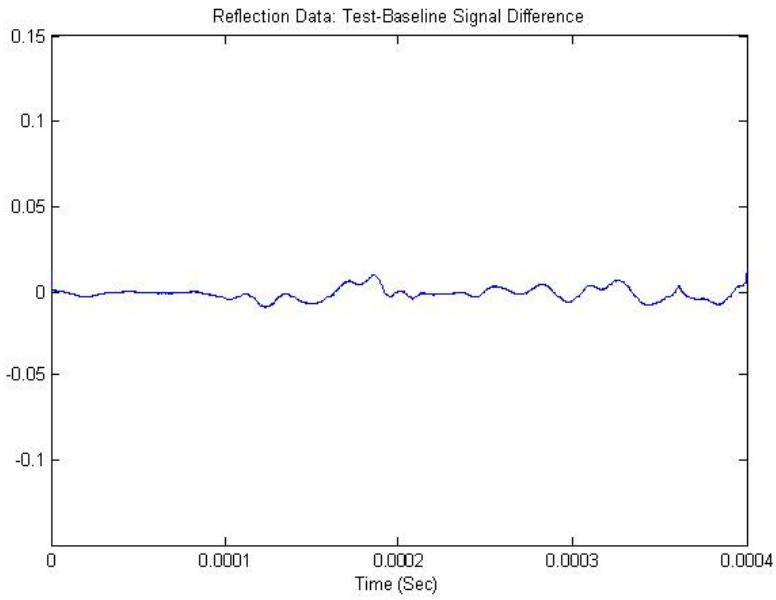

Figure 15: Damage Case 2: Reflected Waves Indistinguishable from Noise.

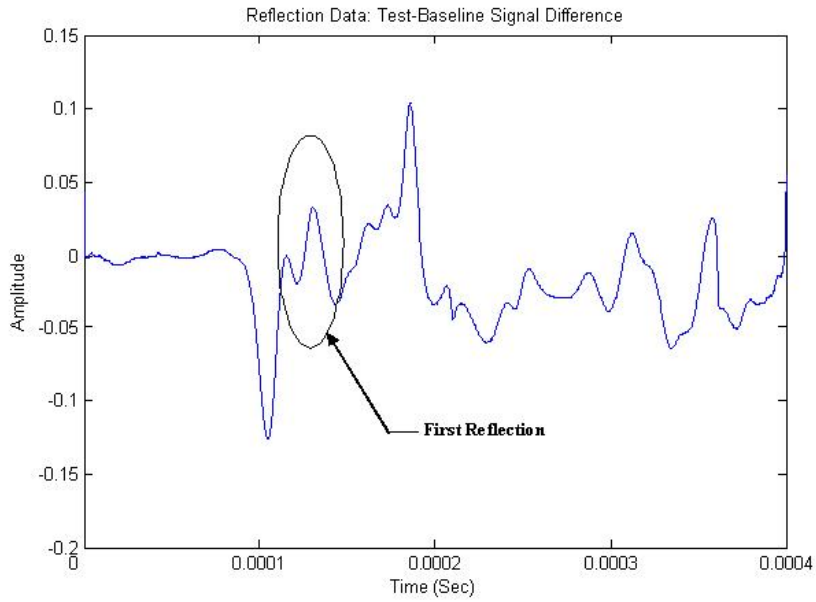

Figure 16: Damage Case 7: Reflected Waves Visible.

There are two primary problems encountered in interrogation of the signal reflections in the honeycomb aluminum panel application. First is the large number of reflections in the signal due to the honeycomb structure. This problem results in a relatively noisy difference signal, making small changes in the condition of the panel difficult to detect. Similarly, the plate boundary reflections also interfere with the damage boundary reflections. More damaging to the ability of the algorithm to identify damage is the anisotropic nature of the panel. It is observed that waves travel with different magnitudes and at different velocities depending on which direction they propagate through the panel. The result of these complications is a very chaotic signal in which many reflections not associated with damage are not satisfactorily cancelled out by the subtraction of the baseline signal from the test signal. The resulting signals are seen to exhibit damage indices that are more dependent on the direction a wave traveled than the presence or absence of any damage, making the full automation of the reflection algorithm for honeycomb aluminum panels nearly impossible as it is proposed.

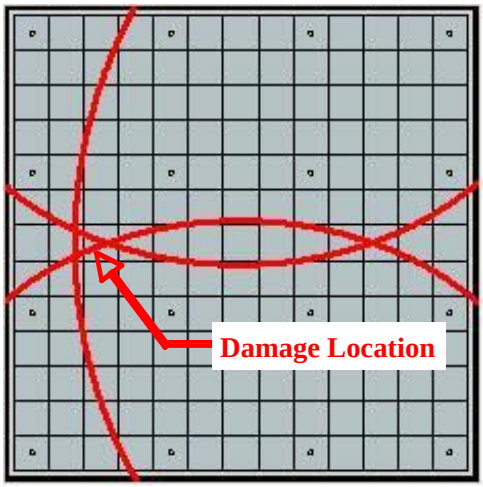

Figure 17: Lamb Wave Triangulation.

4. DISCUSSION

By integrating four signal processing algorithms, a SHM tool has been created that is generic and universal. Because each algorithm is sensitive to different forms of damage in different applications, the side by side comparison of their results provided by the H.O.P.S. GUI is especially effective in allowing the analyst to identify damage. By integrating the software and hardware functions into one package and automating the process, the burden for the analyst is significantly reduced.

By employing a suite of SHM algorithms, H.O.P.S. becomes a useful data interrogation program for a variety of plate structures. In the case of the honeycomb aluminum panels, the different algorithms produce varying degrees of efficacy. The wavelet attenuation analysis is particularly effective in identifying and locating damage. The cross-correlation of power spectral densities is not sensitive to small scale face wrinkling and delamination, however, because the entire received signal is interrogated, it has the potential to be a better tool to characterize the status of the entire system as well as the degree of damage. The reflected wave triangulation technique gives the fastest result using the fewest transducers, but is adversely sensitive to both reflections from the honeycomb structure and the effects of the anisotropic nature of the panel; however, the relative sensitivities of the various components of H.O.P.S. are likely to change for other plate structures in different applications. Although the SHM algorithms are most sensitive to damage on the sensor side of the panel, they are also capable of identifying damage on the opposite side as well.

5. CONCLUSIONS

This study developed an automated and integrated Lamb wave-based active SHM system for plate-like structures. The use of a suite of SHM signal processing algorithms provides the analyst with a richer output than would a single algorithm alone. Future work is required on the H.O.P.S. program to increase the sensitivity of the system and reduce the effects of noise and the complexities of the material. Additional suggested work to improve the program is also warranted. The addition of impedance-based methods [6] would provide another SHM algorithm for comparison as well as provide a means of monitoring the health of the piezoelectric transducers themselves [11]. Further study of environmental effects on the sensitivity of the SHM algorithms is required to implement the system in the real world. Currently, the H.O.P.S. software is configured to run only on a specific hardware configuration; it would be beneficial to reconfigure it to be more flexible and run on a variety of platforms. Finally, to fully realize the potential of the integrated algorithm scheme assembled in H.O.P.S., it is necessary to optimize the SHM algorithms for a greater number of materials, configurations, and damage types that would result in a flexible, easy to use tool for SHM in many types of plate structures.

6. ACKNOWLEDGEMENTS

The authors wish to acknowledge the Engineering Science and Applications Division of the Los Alamos National Laboratory as well as the Critical Skills Program Office in the Department of Energy for funding the Los Alamos Dynamics Summer School. The authors wish to express their gratitude to Scot Hart for early code development. The authors also wish to acknowledge The Mathworks, Inc. for their generous donation of numerical analysis software, and Hibbitt, Karlsson and Sorensen, Inc. for their generous donation of ABAQUS CAE finite element software.

7. REFEREENCES

[1] United States Department of Defense, “Loading, Degradation and Repair of F-111 Bonded Honeycomb Sandwich Panels – Preliminary Study,” Aug. 2000, DSTO-TR-1041, Washington: DoD, pp. 2-5.

[2] United States Government Accounting Office, “Unmanned Aerial Vehicles: Progress of the Global Hawk Advanced Concept Technology Demonstration,” April 2000, GAO/NSIAD-00-78, Washington: GAO, pp. 14.

[3] United States Government Accounting Office, “Unmanned Aerial Vehicles: Major Management Issues Facing DOD's Development and Fielding Efforts,” March 2004, GAO-04-530T, Washington: GAO, pp. 4.

[4] Hundhausen, R. J., Adams, D. E., and Derriso, M. M., “Identification of Damage in a Standoff Metallic Thermal Protection System Panel Subjected to Combined Thermo-Acoustic Excitation,” May 2005, *Proceedings of SPIE: Health Monitoring and Smart Nondestructive Evaluation of Structural and Biological Systems IV*, **5768**, pp. 145-156.

[5] Lee, B. C. and Staszewski, W. J., “Modeling of Lamb Waves for Damage Detection in Metallic Structures: Part I. Wave Propagation,” Oct. 2003, *Smart Materials and Structures*, **12**(5), pp. 804-814.

[6] Kessler, S, S., Spearing, S. M., and Soutis, C., “Structural Health Monitoring in Composite Materials Using Lamb Wave Methods,” April 2002, *Smart Materials and Structures*, **11**, pp. 269-278.

[7] Park, G., Sohn, H., Farrar, C. R., and Inman, D. J., “Overview of Piezoelectric Impedance-based Health Monitoring and Path Forward,” 2003, *The Shock and Vibration Digest,* **35**(6), pp. 451-463.

[8] Sohn, H., Park, G., Wait, J. R., Limback, N. P., Farrar, C. R., “Wavelet-Based Active Sensing for Delamination Detection in Composite Structures,” Feb. 2004, *Smart Materials and Structures*, **13**(1), pp. 153-160.

[9] Abbate, A., Koay, J., Frankel, J., Schroefer, S. C., Das, P., “Signal Detection and Noise Suppression Using a Wavelet Transform Signal Processor: Applications to Ultrasonic Flaw Detection,” 1997, *IEEE Transactions on Ultrasonics, Ferroelectrics, and Frequency Control*, **44**, pp. 14-26.

[10] Lind, R., Kyle, S., Brenner, M., “Wavelet Analysis to Characterize Nonlinearities and Predict Limit Cycles of an Aeroelastic System,” 2001, *Collection of Technical Papers - AIAA/ASME/ASCE/AHS/ASC Structures, Structural Dynamics & Materials Conference* **2**, pp. 337-356.

[11] Park, G., Farrar, C. R., Rutherford, A. C., Robertson, A. N. “Piezoelectric Active Sensor Self-Diagnostics using Electrical Admittance Measurements.” Submitted to *ASME Journal of Vibration and Acoustics*.